CAMBRIDGE
UNIVERSITY PRESS

Article

Langhofite, Pb$_2$(OH)[WO$_4$(OH)], a new mineral from Långban, Sweden

Dan Holtstam[1] (iD), Fernando Cámara[2] (iD) and Andreas Karlsson[1] (iD)

[1]Department of Geosciences, Swedish Museum of Natural History, Box 50007, SE-104 05 Stockholm, Sweden; and [2]Università degli Studi di Milano, Dipartimento di Scienze della Terra 'A. Desio', Via Luigi Mangiagalli 34, 20133, Milano, Italy

Abstract

Langhofite, ideally Pb$_2$(OH)[WO$_4$(OH)], is a new mineral from the Långban mine, Värmland, Sweden. The mineral and its name were approved by the International Mineralogical Association Commission on New Minerals, Nomenclature and Classification (IMA2019-005). It occurs in a small vug in hematite–pyroxene skarn associated with calcite, baryte, fluorapatite, mimetite and minor sulfide minerals. Langhofite is triclinic, space group $P\bar{1}$, and unit-cell parameters $a = 6.6154(1)$ Å, $b = 7.0766(1)$ Å, $c = 7.3296(1)$ Å, $\alpha = 118.175(2)°$, $\beta = 94.451(1)°$, $\gamma = 101.146(1)°$ and $V = 291.06(1)$ Å^3 for $Z = 2$. The seven strongest Bragg peaks from powder X-ray diffractometry are [d_{obs}, Å $(I)(hkl)$]: 6.04(24)(010), 3.26(22)(11$\bar{2}$), 3.181(19)(200), 3.079(24)(1$\bar{1}$2), 3.016(100)(020), 2.054(20)(3$\bar{1}$1) and 2.050(18)(13$\bar{2}$). Langhofite occurs as euhedral crystals up to 4 mm, elongated along the **a** axis, with lengthwise striation. Mohs hardness is *ca.* 2½, based on VHN$_{25}$ data obtained in the range 130–192. The mineral is brittle, with perfect {010} and {100} cleavages. The calculated density based on the ideal formula is 7.95(1) g·cm^{-3}. Langhofite is colourless to white (non-pleochroic) and transparent, with a white streak and adamantine lustre. Reflectance curves show normal dispersion, with maximum values 15.7–13.4% within 400–700 nm. Electron microprobe analyses yield only the metals Pb and W above the detection level. The presence of OH-groups is demonstrated with vibration spectroscopy, from band maxima present at ~3470 and 3330 cm^{-1}. A distinct Raman peak at *ca.* 862 cm^{-1} is related to symmetric W–oxygen stretching vibrations. The crystal structure is novel and was refined to $R = 1.6$%. It contains [W$_2$O$_8$(OH)$_2$]$^{6-}$ edge-sharing dimers (with highly distorted WO$_6$-octahedra) forming chains along [101] with [(OH)$_2$Pb$_4$]$^{6+}$ dimers formed by (OH)Pb$_3$ triangles. Chains configure (010) layers linked along [010] by long and weak Pb–O bonds, thus explaining the observed perfect cleavage on {010}. The mineral is named for curator Jörgen Langhof (b. 1965), who collected the discovery sample.

Keywords: langhofite, new mineral, lead tungsten oxysalt, crystal structure, skarn, Långban, Sweden

(Received 18 February 2020; accepted 21 April 2020; Accepted Manuscript published online: 24 April 2020; Associate Editor: Irina O. Galuskina)

Introduction

Moore ([1970](#)) characterised the Långban deposit in Värmland, Sweden, as "the most remarkable mineral locality on Earth". Although the validity of this statement is ultimately a matter of taste, Långban is still the most prolific ore deposit based on objective criteria, with 73 valid type species, and presently only challenged by Tsumeb (72) (www.mindat.org). A crucial metal contributing to the diversity at Långban is Pb. There are at least 58 Pb minerals present (of which 52 are oxy-compounds) in total, and 31 type minerals with essential Pb. Previously only one Pb–W mineral has been identified with certainty from here; stolzite crystals occur as a rarity, confined to vugs in hematite–garnet skarn (Boström, [1965](#)). Herein, we present another one, langhofite, approved by the International Mineralogical Association (IMA) Commission on New Minerals, Nomenclature and Classification (IMA2019-005, Holtstam *et al.*, [2019](#)). The new mineral is named

for H. Jörgen S. Langhof (b. 1965), presently mineral curator at the Swedish Museum of Natural History, who collected the discovery specimen. Mr. Langhof has been devoted to investigations of the Långban mines and their mineral wealth for more than thirty years. He held the position as director of Långban's Mining Museum 1998–2001. The holotype material, including a polished grain mount, is preserved in the type mineral collections of the Department of Geosciences, Swedish Museum of Natural History, Box 50007, SE-104 05 Stockholm, Sweden, under catalogue label GEO-NRM #20030044.

Occurrence

The Långban Fe–Mn–(Ba–As–Pb–Sb–W–Be–B) deposit, in the Filipstad district (59.85°N, 14.26°E, 215 m a.s.l.) was mined, for Fe (hematite–magnetite) ore, Mn (braunite–hausmannite) ore and dolomitic marble, uninterrupted over the period 1711–1972. The carbonate-hosted, syngenetic Långban-type deposits in the Bergslagen ore region of central Sweden primordially formed from hydrothermal–volcanogenic solutions in a shallow-submarine environment at ~1.9 Ga (Boström *et al.*, [1979](#); Holtstam and Mansfeld, [2001](#)).

Fig. 1. Colour photograph of the langhofite type specimen, GEO-NRM #20030044. Field of view is *ca.* 1.2 cm × 0.8 cm.

Table 1. Reflectance values (%) for langhofite.*

λ (nm)	R_2	R_1	λ (nm)	R_2	R_1
400	15.7	14.6	560	14.0	13.1
420	15.5	14.5	580	13.8	13.0
440	14.9	14.1	**589**	13.7	13.0
460	14.8	13.9	600	13.7	12.9
470	14.6	13.8	620	13.4	12.8
480	14.5	13.6	640	13.4	12.8
500	14.2	13.4	**650**	13.5	12.8
520	14.1	13.3	660	13.6	12.8
540	14.0	13.2	680	13.5	12.7
546	14.0	13.2	700	13.5	12.6

*The reference wavelengths required by the Commission on Ore Mineralogy (COM) are given in bold.
R_2 and R_1 corresponds to maximum and minimum reflectance, respectively, measured in two extinction positions.

Langhofite occurs in the type specimen with baryte and calcite in a small cavity. It is partly overgrown by globular Mn-rich calcite, and tiny opaque specks of sulfides (galena, covellite and chalcocite) occurs on the crystals. Additional microscopic phases present are fluorapatite and mimetite. The host matrix consists of coarse-grained hematite, calcite and green diopside. This specimen was collected on an old (likely accumulated before the year 1900) mine-waste dump close to lake Långban in 2000. A few other samples have been recorded recently, in similar rock matrices.

Magnusson (1930) in his comprehensive geological and mineralogical description of the Långban mines divided the evolution of the deposit into four periods. The early ones, named A and B, correspond to main ore- and skarn-forming processes (B representing regional peak metamorphism), whereas later paragenetic episodes, C and D, refer to mineral formation in vugs and fissures, respectively, at essentially progressively lower temperatures. The C

period is also associated with the appearance of sulfide minerals in the deposit.

The Fe ores in Långban-type deposits are generally enriched in W (sequestered by scheelite; Holtstam, 2001) whereas Pb is, in the present case, most likely to have been mobilised from Mn-rich lithologies, where a number of Pb silicate and arsenate minerals occur in the skarns (Nysten *et al.*, 1999). Fluid-inclusion studies of mineral assemblages with Pb oxysalts of the D period suggest formation temperatures ≤180°C and nearly atmospheric pressure conditions (Jonsson and Broman, 2002). We believe that langhofite has formed well below peak metamorphic conditions at Långban (estimated at >600°C and <3.5 kb; Grew *et al.*, 1994; Christy and Gatedal, 2005), but still above the estimated temperature maximum for the D period, i.e. probably in the range 200−400°C. Mineral formation probably took place in an alkaline environment, but not at such extreme high-pH conditions that are inferred to have prevailed in the
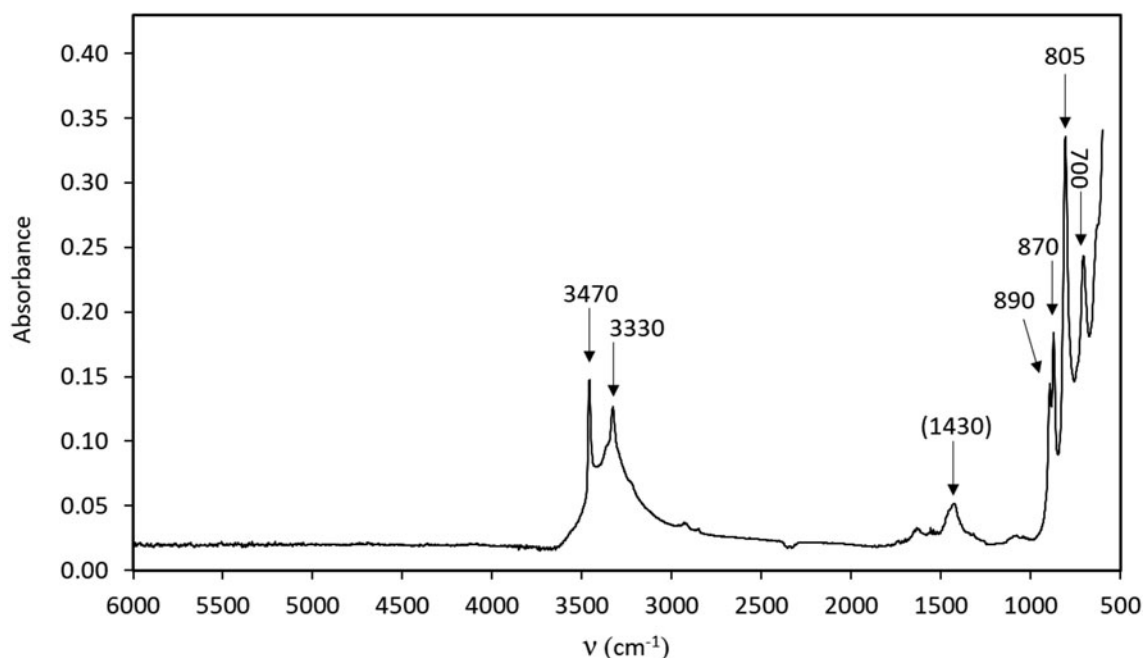
Fig. 2. FTIR spectrum (powder sample with KBr) of langhofite. The broad band at *ca.* 1430 cm^{-1} is related to a carbonate impurity.
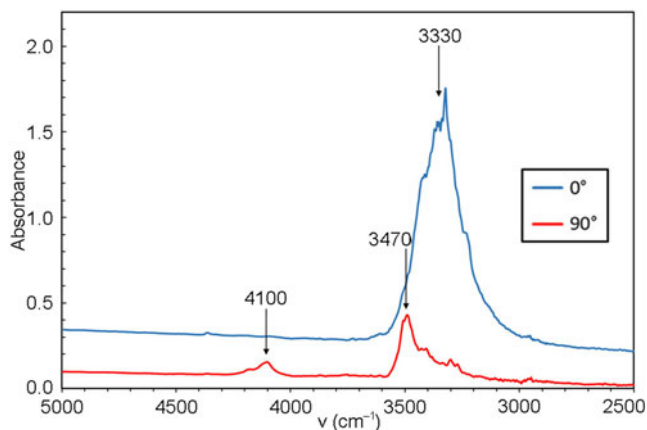
Fig. 3. Polarised FTIR spectra (single crystal in two mutually perpendicular directions, ~70 μm sample thickness).

'reduced veins' characteristic for the late-stage D period at Långban (Boström, 2002).

Physical and optical properties

The new mineral occurs in a single aggregate, *ca.* 10 mm × 5 mm, of several crystals (Fig. 1) on the type specimen. Individual crystals are euhedral, elongated along **a**, up to 4 mm in greatest dimension, somewhat flattened on {001} and striated lengthwise. Langhofite is white to colourless, with white streak; lustre is adamantine. Fluorescence effects are absent under both long- and short-wave ultraviolet radiation. The mineral is brittle

under compression, with uneven, splintery fracture. Cleavage is perfect in two directions, {010} and {100}, producing rhombic cleavage fragments.

The density of langhofite is undetermined owing to the fragile nature of the crystals and high anticipated value ($>4.2 \text{ g·cm}^{-3}$). The calculated density, from the unit-cell dimensions and atom content (ideal formula), is 7.95(1) g·cm^{-3}. Vickers hardness numbers (VHN_{25}) were obtained using a Shimadzu type-M microhardness tester; the average of nine indentation measurements is 157 (range 130–192), which corresponds to 2½–3 on Mohs' scale.

Optically, langhofite is biaxial (+) and non-pleochroic in transmitted light. Refractive indices were not measured conventionally, because it was found to be higher than available reference liquids (>1.9); a value of 2.20 is predicted from Gladstone–Dale constants (Mandarino, 1981). Polarised reflectance spectra were measured in air with an AVASPEC-ULS2048×16 spectrometer attached to a Zeiss Axiotron UV-microscope (10×/0.20 Ultrafluar objective), using a halogen lamp (100 W) and a SiC (Zeiss no. 846) standard, with a circular sample measurement field of 120 μm in diameter. The results from the 400–700 nm range (average of 1000 scans, 10 ms integration time) are given in Table 1. Calculated refractive indices from the reflectance data using Fresnel's equation (assuming zero absorption in the crystals) are $n_2 = 2.20(2)$ and $n_1 = 2.14(2)$ at 546 nm.

Infrared and Raman spectroscopy

A Fourier-transform infrared (FTIR) spectrum (Fig. 2) was collected on powder (~1 mg) mixed with KBr in the range 6000–600 cm^{-1} at a spectral resolution of 4 cm^{-1}, with a Bruker Vertex 70 spectrometer attached to a Bruker Hyperion 2000 IR-microscope. In the 1000–600 cm^{-1} range, sharp absorption
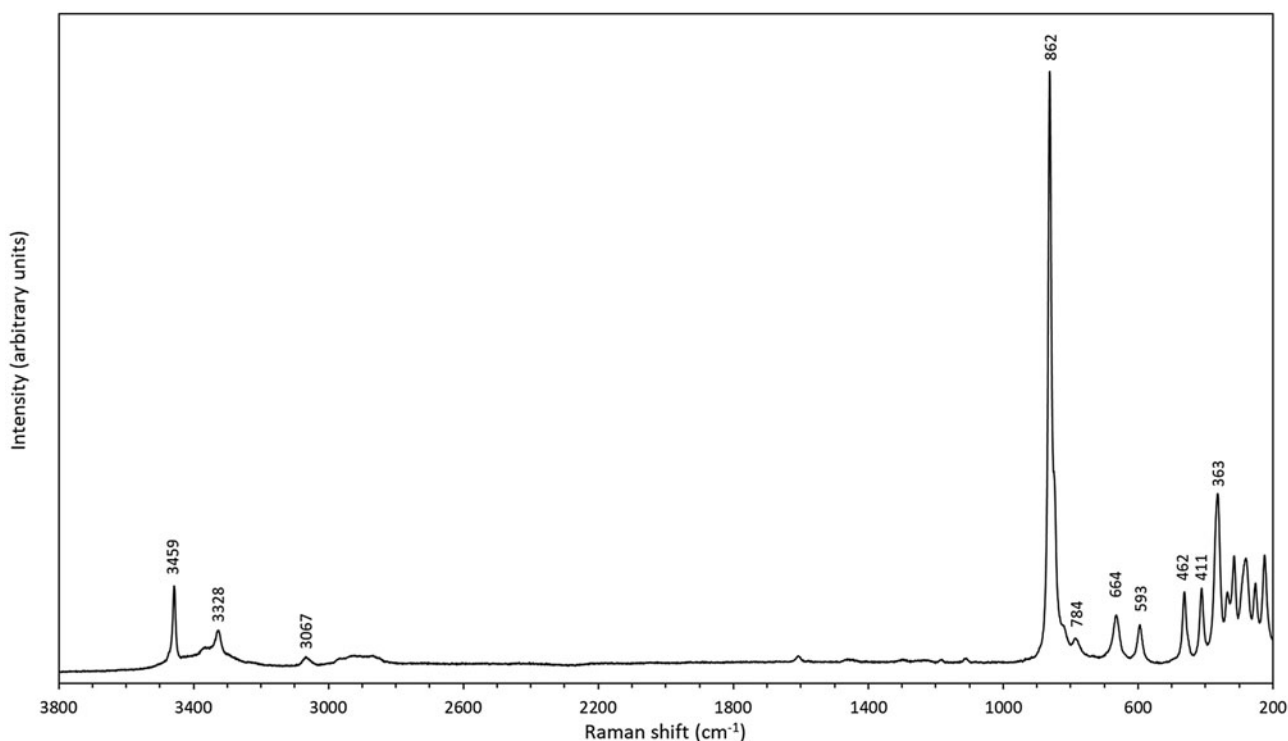

Fig. 4. Raman spectrum of langhofite, random section.

Table 2. X-ray powder diffraction data (*d* in Å) for langhofite

I_{meas} (%)	I_{calc} (%)	d_{obs}	d_{calc}	*h k l*
2	11	6.35	6.36	100
5	29	6.16	6.15	01$\bar{1}$
24	30	6.04	6.02	010
4	25	5.10	5.09	1$\bar{1}$0
2	8	5.00	5.00	10$\bar{1}$
2	14	4.60	4.61	1$\bar{1}$1
3	10	4.26	4.26	11$\bar{1}$
7	42	4.10	4.11	101
7	35	3.891	3.893	110
11	31	3.568	3.568	011
2	3	3.471	3.470	02$\bar{1}$
17	73	3.330	3.332	1$\bar{2}$1
22	100	3.259	3.260	11$\bar{2}$
19	51	3.181	3.181	200
16	35	3.094	3.096	20$\bar{1}$
24	94	3.0788	3.0789	1$\bar{1}$2
100	86	3.0156	3.0111	020
4	5	2.8111	2.8098	111
13	44	2.7640	2.7669	$\bar{2}$11
3	10	2.7405	2.7396	21$\bar{1}$
7	25	2.6878	2.6887	12$\bar{2}$
4	21	2.6396	2.6374	102
11	32	2.5483	2.5499	210
2	8	2.4820	2.4807	21$\bar{2}$
12	39	2.4165	2.4183	$\bar{1}$12
2	3	2.3878	2.3906	$\bar{1}$21
3	8	2.3604	2.3611	012
2	3	2.3104	2.3103	021
12	32	2.2669	2.2681	1$\bar{3}$2
1	3	2.2302	2.2303	12$\bar{3}$
4	7	2.1733	2.1717	$\bar{2}$21
6	8	2.1450	2.1454	22$\bar{1}$
9	18	2.1315	2.1329	10$\bar{3}$
4	6	2.0832	2.0816	$\bar{3}$11
20	30	2.0535	2.0548	3$\bar{1}$1
18	18	2.0498	2.0509	13$\bar{2}$
8	6	2.0090	2.0074	030
5	11	1.9913	1.9905	3$\bar{2}$1
7	12	1.9468	1.9468	30$\bar{2}$
3	7	1.8893	1.8887	2$\bar{2}$3
7	27	1.8261	1.8249	02$\bar{4}$
11	8	1.7841	1.7847	130
4	4	1.7538	1.7535	$\bar{1}$31
3	4	1.7343	1.7349	04$\bar{2}$
6	13	1.7113	1.7114	1$\bar{4}$1
10	9	1.6916	1.6910	31$\bar{3}$
13	16	1.6861	1.6855	32$\bar{2}$

bands seen at 890, 870, 805 and 700 cm^{-1} are related to metal–oxygen interactions. A broad band at ~1430 cm^{-1} is ascribed to a carbonate impurity in the powder absorber.

A crystal fragment of *ca.* 70 µm thickness attached to a glass plate was measured with the same instrument using polarised light in the range 5000–2000 cm^{-1} for two vibration directions, approximately along and perpendicular to the elongation direction, of the crystal, respectively (Fig. 3). In the 4000–3000 cm^{-1} range of both types of spectra (powder and single crystal), two distinct absorption bands are identified at *ca.* 3470 and 3330 cm^{-1}. Based on structural data (see paragraph below) these are assigned to the O–H stretching modes of two protonated O sites. A band visible in only one of the directions at 4100 cm^{-1} is probably related to metal–OH motions.

Micro-Raman measurements were performed at room temperature using a Horiba (Jobin Yvon) LabRam HR Evolution. An unoriented polished crystal was excited with an air-cooled frequency doubled 532 nm Nd-YAG laser with an Olympus

100× objective (numerical aperture = 0.9). Spectra were generated in the range of 4000 to 25 cm^{-1} utilising a 600 grooves/cm grating. The spectral resolution was in the order of 1 cm^{-1} and the lateral resolution was ~1 µm. The wavenumber calibration was done using the 520.7 cm^{-1} Raman band on a polished silicon wafer with a wavenumber accuracy usually better than 0.5 cm^{-1}. The spectrum shown (Fig. 4) was collected through 10 acquisition cycles with single counting times of 30 s in a close to back-scattered geometry. Two distinct peaks, corresponding to the OH bands in the FTIR spectrum, occur at 3459 and 3328 cm^{-1} (with a third one at 3070 cm^{-1} and a broad weak band centred at *ca.* 2900 cm^{-1}). In the 900–350 cm^{-1} region, distinct Raman bands are seen at 862 (with a shoulder at ~850), 784, 664, 593, 462, 411 and 363 cm^{-1}. The strongest peak at 862 cm^{-1} is ascribable to the symmetric W–O stretching vibrations of the WO$_6$-octahedra, also found in related raspite (Bastians *et al.*, 2004; Yang and Huang, 2012) at 870 cm^{-1}. The corresponding absorption in the IR spectrum of langhofite is at 870 cm^{-1} and of raspite at 874 cm^{-1} (Chukanov, 2014).

Chemical composition

Preliminary energy-dispersion X-ray (EDS) measurements showed only Pb, W and O in langhofite. A more precise determination of the composition was made from eight point analyses on a polished surface using a JEOL 8200 Super Probe (accelerating voltage 15 kV, sample current 5 nA, beam size 1 µm, counting time 30 s in peak and 10 s on the background positions) in wavelength dispersion (WDS) mode, with the reference materials galena (Pb*M*α) and pure metal (W*L*α). Mo was analysed for, but found close to or below the detection limit. No other elements were detected in WDS spectrometer scans. H$_2$O was not determined quantitatively, because of a dearth of material. The results (in wt.%) of the analyses, done on the crystal used for the single-crystal study (see below) are: PbO 63.51 (range 62.61–64.52), WO$_3$ 32.01 (31.35–32.40), H$_2$O$_{calc}$ 2.52, total 98.04. The empirical composition is Pb$_{2.03}$W$_{0.99}$O$_4$(OH)$_2$ based on six O atoms per formula unit. The simplified formula is Pb$_2$WO$_4$(OH)$_2$ and the ideal structural formula can be written as Pb$_2$(OH)[WO$_4$(OH)]; both require (in wt.%) PbO 64.11, WO$_3$ 33.30, H$_2$O 2.59, total 100.00.

X-ray diffraction data and crystal-structure refinement

Powder X-ray diffraction data were recorded on a PANalytical X'Pert[3] Powder diffractometer equipped with an X'celerator silicon-strip detector and operated at 40 mA and 45 kV (Cu*K*α-radiation, λ = 1.5406 Å). Bragg peak positions were determined with the PANalytical *HighScore Plus 4.6* software and corrected against an external Si standard (NBS 640b). Indexed *d* values and relative peak-heights above background are given in Table 2. The triclinic unit-cell parameters, obtained by least-squares refinement of forty-seven reflections, are *a* = 6.6118(3) Å, *b* = 7.0748(4) Å, *c* = 7.3264(4) Å, α = 118.125(6)°, β = 94.503(5)°, γ = 101.146(5)° and *V* = 290.79(3) Å^3 for *Z* = 2.

A single-crystal X-ray study was done on a 146 µm × 90 µm × 10 µm crystal fragment (flat on (010)) using an Rigaku Oxford Diffraction XtaLAB Synergy diffractometer, with a PhotonJet X-ray source operating at 50 kV and 1 mA, with monochromatised Mo*K*α radiation and equipped with a Hybrid Pixel Array detector (HyPix) at 62 mm from the sample position. A combination of 32 ω scans for 6570 images, with step scan 0.5° and

Table 3. Data and experimental details for single-crystal X-ray diffraction study of langhofite.

Crystal data	
Ideal formula	$Pb_2(OH)[WO_4(OH)]$
Crystal dimensions (mm)	$0.146 \times 0.090 \times 0.010$
Crystal system, space group	Triclinic, $P\bar{1}$
Temperature (K)	293(2)
a, b, c (Å)	6.6154(1), 7.0766(1), 7.3296(1)
α, β, γ (°)	118.175(2), 94.451(1), 101.146(1)
V (Å^3)	291.06(1)
Z	2
Calculated density (g·cm^{-3})	7.95(1)
μ (mm^{-1})	77.371
Data collection	
Crystal description	Colourless lath
Instrument	Rigaku Oxford Diffraction XtaLAB Synergy
Radiation type, wavelength (Å)	Mo$K\alpha$, 0.71073
Number of frames	6570
θ range (°)	3.20 to 40.43
Absorption correction	Multiscan (SCALE3 ABSPACK, Rigaku Oxford Diffraction ®)
T_{min}, T_{max}	0.028, 1
Number of measured, independent and observed reflections	29035, 3647, 3360
R_{int}	0.040
Data completeness to 40.43° (%)	99.4
Indices range of h, k, l	$-12 \leq h \leq 11, -12 \leq k \leq 12, -13 \leq l \leq 13$
Refinement	
Refinement method	Full-matrix least-squares on F^2
Number of reflections, parameters, restraints	3647, 86, 0
R_1 [$I > 2\sigma(I)$], R_2 (all)	0.0163, 0.0190
GoF	1.034
wR_1 [$I > 2\sigma(I)$], wR_2 (all) *	0.0374, 0.0366
No. of refined parameters	86
Extinction coefficient	0.00294(14)
$\Delta\rho_{max}$, $\Delta\rho_{min}$ (e^- Å^{-3})	1.892, −1.515

* Weighting scheme: $w = 1/[\sigma^2(F_o^2)+(0.0187P)^2]$, where $P=(F_o^2+2F_c^2)/3$

Table 4. Fractional atomic coordinates, thermal parameters and bond-valence sums (BVS) of langhofite.

Site	W*		Occ.	x/a	y/b	c/z	U_{eq}/U_{iso}	BVS**
Pb1	2i	Pb	1	0.35798(2)	0.22210(2)	0.48875(2)	0.01868(3)	2.125
Pb2	2i	Pb	0.9983(8)	0.26698(2)	0.29219(2)	1.00803(2)	0.01748(3)	2.113
W	2i	W	0.9964(9)	0.82374(2)	0.31638(2)	0.28718(2)	0.01304(3)	5.832
O1	2i	O	1	0.1940(3)	0.8502(4)	0.9873(3)	0.0197(4)	1.798
O2	2i	O	1	0.8806(3)	0.5872(4)	0.6248(3)	0.0161(3)	1.912
O3	2i	O	1	0.7674(3)	0.1137(4)	0.3672(3)	0.0203(4)	1.839
O4	2i	O	1	0.5601(3)	0.3865(4)	0.3013(3)	0.0158(3)	2.180
OH1	2i	O	1	0.1187(3)	0.3768(4)	0.7379(3)	0.0181(3)	1.077
OH2	2i	O	1	0.5635(3)	0.3291(4)	0.8275(3)	0.0181(3)	1.263
H2	2i	H	1	0.6841	0.2985	0.8469	0.022	

*W = Wyckoff position; ** BVS = Bond-valence sum and bond-valence parameters from Gagné and Hawthorne (2015).

exposure time 2.4/8.4 s per frame (depending on θ angle) were used to maximise redundancy and data coverage.

The crystal structure was solved using charge-flipping methods with *SUPERFLIP* (Palatinus and Cahpuis, 2007) implemented in *JANA2006* (Petříček *et al.*, 2014). The experimental data are summarised in Table 3. The structure was refined by least squares minimisation using *SHELXL-2018/3* (Sheldrick, 2015). At convergence, with a model employing anisotropic displacement parameters, it was possible to locate one of the two protons in the structure, found close to the OH2 anion site. The position of this proton atom (H2) was added to the model and the isotropic displacement value was constrained to $1.2 \times$ the U_{eq} value refined at the OH2 site, following a riding model. The coordinates obtained at the Fourier-difference map were kept fixed as they

yield unreasonable values if refined. The geometry of the hydrogen bonding is discussed below. Atomic coordinates, equivalent isotropic displacement parameters and calculated bond valences are given in Table 4. Bond distances are reported in Table 5. Anisotropic displacement parameters are reported in the crystallographic information file that has been deposited with the Principal Editor of *Mineralogical Magazine* and is available as Supplementary material (see below).

Description of the crystal structure

The structure of langhofite contains three cation sites: there are two unique Pb positions, Pb1 and Pb2, (4 + 4)-coordinated to O, and one W site. The W site is coordinated to five oxygen
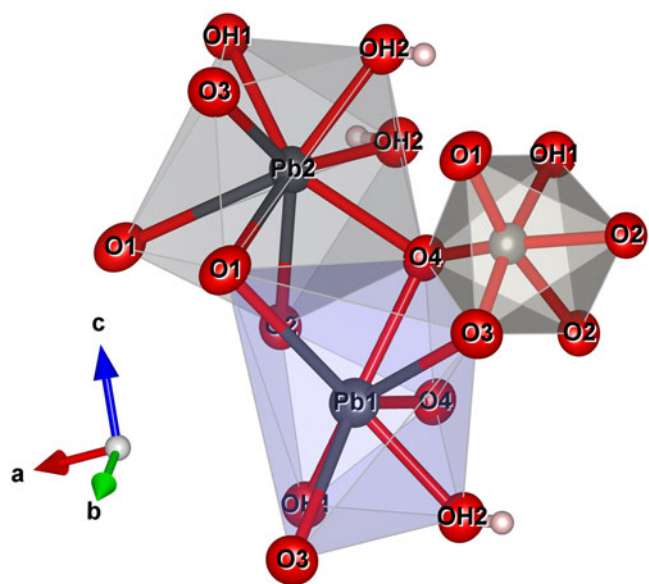
Table 5. Selected bond distances (Å) and angles (°) for langhofite.

W–O1	1.767(2)	Pb1–O4	2.368(2)	Pb2–OH2	2.339(2)
W–O3	1.778(4)	Pb1–OH2	2.427(2)	Pb2–OH2	2.490(2)
W–O2	1.892(2)	Pb1–O4	2.495(2)	Pb2–OH1	2.507(1)
W–O4	1.901(3)	Pb1–OH1	2.504(2)	Pb2–O4	2.515(2)
W–OH1	2.227(4)	Pb1–O2	2.585(2)	Pb2–O2	2.736(2)
W–O2	2.244(2)	Pb1–O3	3.032(2)	Pb2–O3	2.838(1)
<W–O>	1.965	Pb1–O3	3.042(2)	Pb2–O1	2.999(3)
V (Å^3)	9.65	Pb1–O1	3.280(3)	Pb2–O1	3.029(2)
OQE*	1.046	<Pb1–O>	2.716	<Pb2–O>	2.682
OAV* (°^{2})	118.73	V (Å^3)	33.95	V (Å^3)	32.37

Hydrogen bonding

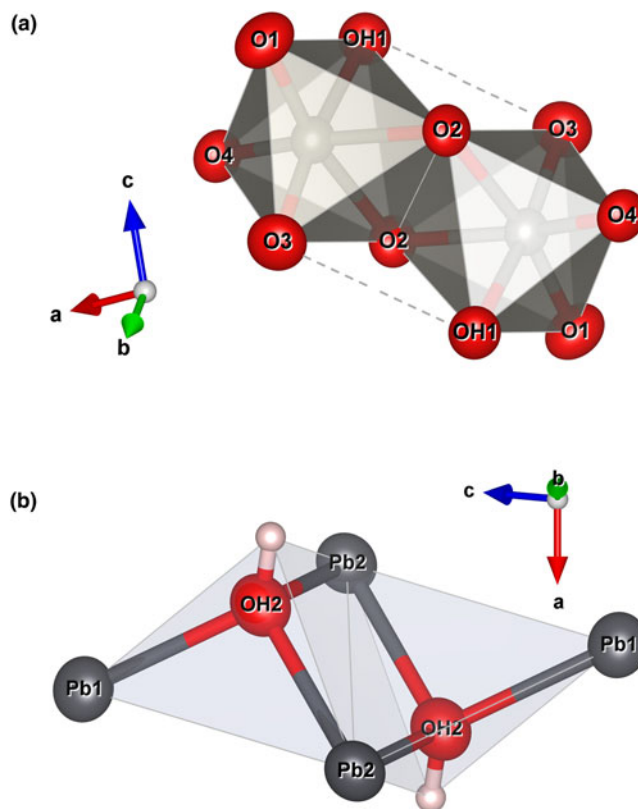| Bond	$D \cdots A$ (Å)	D–H (Å)	H$\cdots A$ (Å)	<DHA (°)
OH1–O3	2.970(3)			
OH2–O1	2.846(2)	0.884(2)	2.149(1)	135.3(2)

* OQE = Octahedral quadratic elongation and OAV = Octahedral angle variance in the sense of Robinson *et al.* (1971).
D = donor O; *A* = acceptor O.

Fig. 6. Polyhedral representation of the $[W_2O_8(OH)_2]^{6-}$ (*a*) and $[(OH)_2Pb_4]^{6+}$ (*b*) dimers. Drawn with *Vesta 3.0* (Momma and Izumi, 2011).

Fig. 5. The coordination environment of the two Pb sites and the W site in the structure of langhofite. The stronger (shorter) bonds are shown in red. Drawn with *Vesta 3.0* (Momma and Izumi, 2011).

atoms and one (OH) group. It is strongly deformed (octahedral angle variance (OAV) = 118.73°^{2}; Robinson *et al.* 1971), having two very short (<1.78 Å), two intermediate (*ca.* 1.90 Å) and two long distances (*ca.* 2.23 Å), of which one is to the (OH) group. The coordination polyhedra of the Pb atoms are significantly deformed, with Pb^{2+} off-centred toward four anions sites showing shorter distances (Table 5), and three significantly longer (>2.8 Å) distances involving the anion sites participating in the short W–O bonds (O1 and O3) (Fig. 5).

Bond balance incidence at cation sites confirm the expected charge for these sites. Bond-valence sums at the anion sites show: (1) two sites with values <1.27 valence units (OH1 and OH2 sites) and thus identified as (OH)-groups; (2) two slightly undersaturated sites (*ca.* 1.82 valence units for O1 and O3), even if involved in short W–O bonds; (3) one site close to the expected value (O2); and finally, (4) one site (O4) showing a

bond valence incidence higher than expected (probably due to the high coordination number, 4, and three short bonding distances to Pb^{2+} cations).

The crystal structure of langhofite can be described in terms of the stronger bonds. Those are found in the highly distorted WO$_5$(OH)-octahedra, which form $[W_2O_8(OH)_2]^{6-}$ edge-sharing dimers (Fig. 6a). In addition, oxygen atoms at the OH2 site forms three very strong bonds with Pb atoms, thus forming (OH)Pb$_3$ triangles. Two (OH)Pb$_3$ share an edge and thus form a $[(OH)_2Pb_4]^{6+}$ dimer (inset in Fig. 6b).

Both the $[W_2O_8(OH)_2]^{6-}$ and $[(OH)_2Pb_4]^{6+}$ units link, forming chains along [101] (Fig. 7a). The chains configure (010) layers when long Pb–O bonds are also considered (Fig. 7b). The (010) layers link along [010] through the longer and weaker Pb–O bonds, thus explaining the observed perfect cleavage on {010} (Fig. 8).

Hydrogen bonding

Close to one of the two undersaturated oxygen sites, a residual electron density has been detected at a distance of 0.88 Å, thus corresponding to the plausible location of a proton of an (OH) group. Even if a very thin crystal was used for data collection and a high redundancy of reflections was collected to account for absorption correction, the high absorption coefficient (77.371 mm^{-1}) and the huge scattering contrast between the metal cations and the protons make the localisation of hydrogen atoms difficult. However, considering the O–O distances, it can be observed easily that both OH1 and OH2 have shorter distances (<3 Å) compared to the O1 and O3 anion sites which are slightly
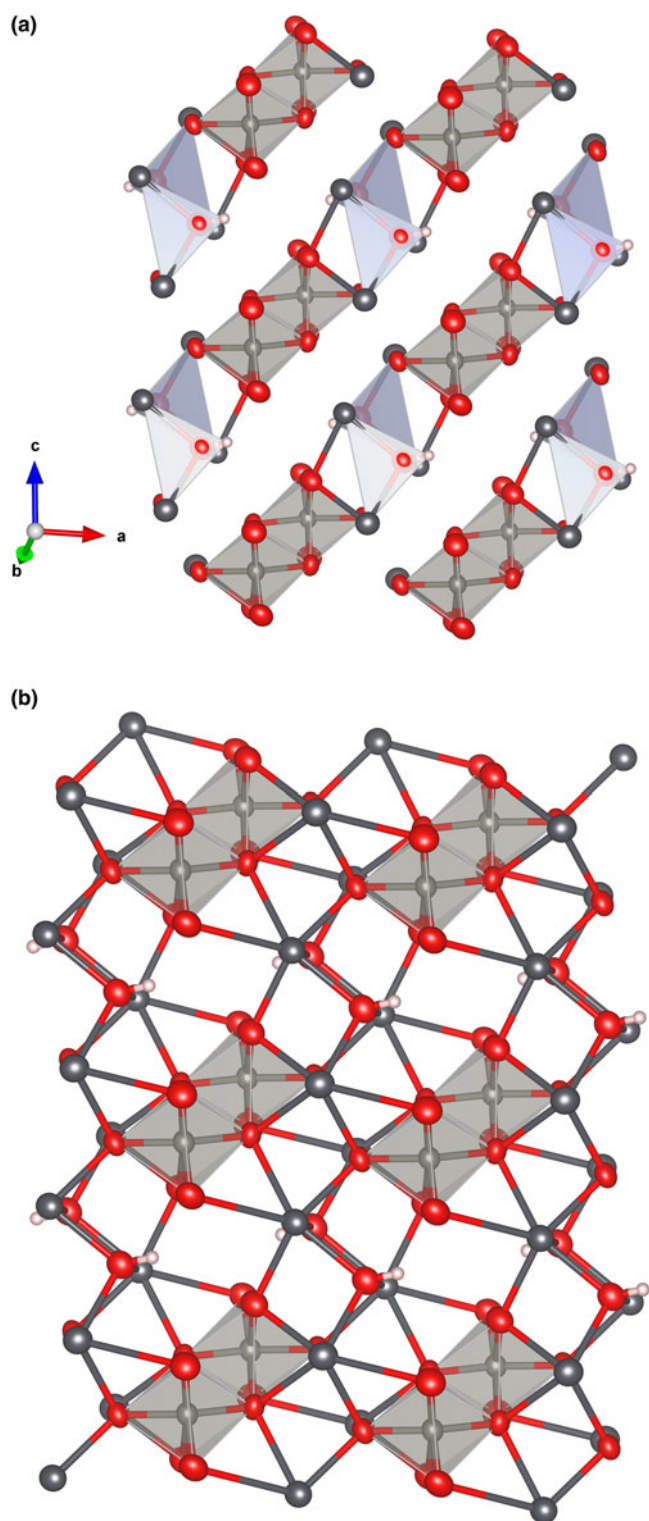
Fig. 7. The $[W_2O_8(OH)_2]^{6-}$ and $[(OH)_2Pb_4]^{6+}$ units forming chains along [101] in langhofite (*a*). The chains configure (010) layers when all the strong Pb–O bonds are considered (*b*). Drawn with *Vesta 3.0* (Momma and Izumi, 2011).

undersaturated and thus ready to act as hydrogen bond acceptors. These short distances occur across the cavities alternating with $WO_5(OH)$ dimers along **c** and cross each other, thus explaining the polarisation behaviour observed for FTIR spectra for the bands at 3470 and 3330 cm^{-1}. Using the empirical calibration of

Libowitzky (1999), the expected positions, based on the O···O distances, for these two bands are 3540 and 3458 cm^{-1}, respectively. This is in reasonable agreement with the observations, considering that the located position of hydrogen at the H2 site is off the O1···OH2 line and thus represent a bent H bond. Bent hydrogen bonds are described by Libowitzky (1999) as a possible reason for outliers in relation to the calibration curve. An increase of up to 70 cm^{-1} would then be due to the bending of the bond, thus correcting the calculated value for O1···OH2, in perfect agreement with the value observed in the FTIR spectra for one of the bands. It is expected that the OH1–H2 bond is also bent. There is no structural indication of H_2O molecules in langhofite.

Relation with other species

In terms of mineral classification, langhofite fits in the Strunz group 04.FD (oxides-hydroxides with OH, without H_2O; chains of edge-sharing octahedra). Of the few other chemically related minerals, belonging to other Strunz groups, stolzite (tetragonal $PbWO_4$; a tungstate) and pinalite ($Pb_3WO_5Cl_2$, oxyhalide, Grice and Dunn, 2000) have different anion coordination figures around the W^{6+} cation (four-fold for stolzite and five-fold for pinalite, respectively).

Considering instead the $(OH)Pb_3$ triangles, these are present in other oxysalts and in some mineral species share vertex forming chains like in penfieldite ($Pb_2Cl_3(OH)$, Merlino *et al.*, 1995) where the chains develop along [001], or sharing edges forming infinite chains like in laurionite ($PbCl(OH)$, Köchlin 1887; Venetopoulos and Rentzeperis 1975) where $(OH)Pb_3$ triangles share edges and form chains along [010]. Sharing of edges by $(OH)Pb_3$ triangles is also observed in Pb oxysalt minerals like in bideauxite ($Pb_2AgCl_3F(OH)$, Cooper *et al.*, 1999) or siidraite ($Pb_2Cu(OH)_2I_3$, Rumsey *et al.*, 2017), where the triangle clusters form cubane-like $[Pb_4(OH)_4]^{4+}$ units. Interestingly, pinalite also has $(OH)Pb_3$ triangles sharing edges between themselves and with WO_5 pyramids, configuring layers alternating with Cl atoms.

Concluding remarks

The crystal structure of langhofite, the only known Pb–W–O–H mineral without other cations, is of a novel type in Nature, showing $[W_2O_8(OH)_2]^{6-}$ dimeric anions between a 3D framework of PbO_8 polyhedra. Similar structural elements (edge-sharing WO_6-octahedra), however, occur in raspite (monoclinic $PbWO_4$; Fujita *et al.*, 1977; Andrade *et al.*, 2014). The WO_6 polyhedron is more distorted in langhofite (Table 5) than found for end-member raspite (from the OAV and quadratic elongation of 118.7°^{2} *vs.* 104°^{2} and 1.045 *vs.* 1.038, respectively; Andrade *et al.*, 2014). The slightly longer average W–O bond in langhofite provides an explanation for the lower W–O stretching frequency observed (with Raman peaks at 863 and 870 cm^{-1}, respectively).

Interestingly, the structure of langhofite is closely related to that of synthetic Pb_3WO_6 (Wang *et al.*, 2012). In this structure, an additional lead atom is placed in the cavities containing protons in langhofite, passing from $Pb_2WO_4(OH)_2$ to Pb_3WO_6 through the substitution PbH_{-2}. Synthetic Pb_3WO_6 was grown in hydrothermal experiments at $T = 300$°C and $P = 600$–800 bars, thus under similar conditions as inferred for langhofite (i.e. 200–400°C and <3.5 kbar). The protonation of langhofite must be ascribed to a milder alkalinity of the fluids as Pb_3WO_6 was grown in aqueous solution of NaOH (3.0 mol/l; Wang *et al.*, 2012). The exchange of Pb by two protons leads to a strain in the structure that goes from triclinic $P\bar{1}$ to monoclinic $P2_1/n$
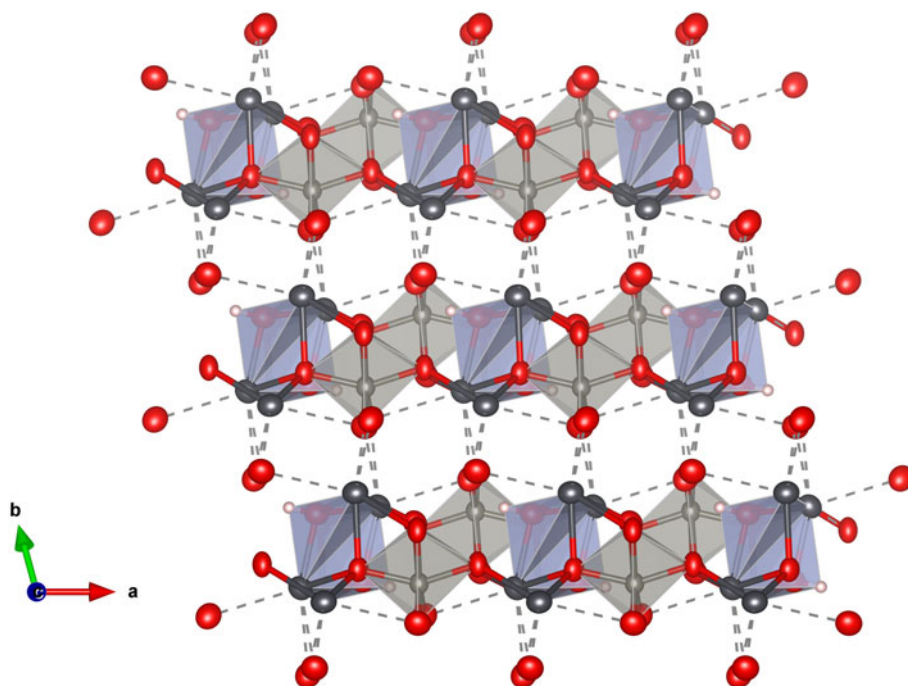
Fig. 8. The layered structure of langhofite: the (010) layers are linked along [010] through the weaker longer Pb–O bonds (shown with dashed lines). Drawn with *Vesta 3.0* (Momma and Izumi, 2011).

symmetry. This relaxation is also observed in the geometry of the W site that, whereas still showing a short distance [W–O4 = 1.770(8) Å], is certainly less deformed (OAV = 72°²). The W^{6+}–W^{6+} distance within the $[W_2O_{10}]^{8-}$ dimer is 3.341(1) Å, even longer than within the $[W_2O_8(OH)_2]^{6-}$ dimer in langhofite, 3.286(1) Å.

References

Andrade M.B., Yang H., Downs R.T., Jenkins R.A. and Fay I. (2014) Te-rich raspite, $Pb(W_{0.56}Te_{0.44})O_4$, from Tombstone, Arizona, USA: The first natural example of Te^{6+} substitution for W^{6+}. *American Mineralogist*, **99**, 1507–1510.

Bastians S., Crump G., Griffith W.P. and Withnall R. (2004) Raspite and studtite: Raman spectra of two unique minerals. *Journal of Raman Spectroscopy*, **35**, 726–731.

Boström K. (1965) The occurrence of senarmontite, stolzite, cuprite and brandtite at Långban. *Arkiv för Mineralogi och Geologi*, **3**, 573–576

Boström K. (2002) Late hydrothermal events at Långban – how many and how alkaline? *GFF*, **124**, 236–237.

Boström K., Rydell H. and Joensuu O. (1979) Långban – An exhalative sedimentary deposit? *Economic Geology*, **74**, 1002–1011.

Christy A.G. and Gatedal K. (2005) Extremely Pb-rich rock-forming silicates including a beryllian scapolite and associated minerals in a skarn from Långban, Värmland, Sweden. *Mineralogical Magazine*, **69**, 995–1018.

Chukanov N.V. (2014) *Infrared Spectra of Mineral Species: Extended Library.* Springer, Dordrecht, 1726 pp.

Cooper M.A., Hawthorne F.C., Merlino S., Pasero M. and Perchiazzi N. (1999) Stereoactive lone-pair behavior of Pb in the crystal structure of bideauxite: $Pb_2AgCl_3F(OH)$. *The Canadian Mineralogist*, **37**, 915–921.

Fujita T., Kawada I. and Kato K. (1977) Raspite from Broken Hill. *Acta Crystallographica*, **B33**, 162–164.

Gagnè O.C. and Hawthorne F.C. (2015) Comprehensive derivation of bond-valence parameters for ion pairs involving oxygen. *Acta Crystallographica*, **B71**, 562–578.

Grew E.S., Yates M.G., Belakovskiy D.I., Rouse R.C., Su S.C. and Marquez N. (1994) Hyalotekite from reedmergnerite-bearing peralkaline pegmatite, Dara-i-Pioz, Tajikistan and from Mn skarn, Långban, Värmland, Sweden: A new look at an old mineral. *Mineralogical Magazine*, **58**, 285–297.

Grice J.D. and Dunn P.J. (2000) Crystal-structure determination of pinalite. *American Mineralogist*, **85**, 806–809.

Holtstam D. (2001) W and V mineralization in Långban-type Fe–Mn deposits: epigenetic or syngenetic? *GFF*, **123**, 29–33.

Holtstam D. and Mansfeld J. (2001) Origin of a carbonate-hosted Fe-Mn-(Ba-As-Pb-Sb-W) deposit of Långban-type in Central Sweden. *Mineralium Deposita*, **36**, 641–657.

Holtstam D., Cámara F. and Karlsson A. (2019) Langhofite, IMA 2019-005. CNMNC Newsletter No. 49: *Mineralogical Magazine*, **83**, 323–328.

Jonsson E. and Broman C. (2002) Fluid inclusions in late-stage Pb-Mn-As-Sb mineral assemblages in the Långban deposit, Bergslagen, Sweden. *The Canadian Mineralogist*, **40**, 47–65

Köchlin R. (1887) Ueber Phosgenit und ein muthmasslich neues Mineral vom Laurion, *Annalen des K.K. Naturhistorischen Hofmuseums*, **2**, 185–190.

Libowitzky E. (1999) Correlation of O–H stretching frequencies and O–H···O hydrogen bond lengths in minerals. *Monatshefte für Chemie*, **130**, 1047–1059.

Magnusson N.H. (1930) Långbans malmtrakt. *Sveriges Geologiska Undersökning*, Ca **23**, 1–111.

Mandarino J.A. (1981) The Gladstone-Dale relationship; Part IV, The compatibility concept and its application. *The Canadian Mineralogist*, **19**, 441–450.

Merlino S., Pasero M., Perchiazzi N. and Gianfagna A. (1995) X-ray and electron diffraction study of penfieldite: average structure and multiple cells. *Mineralogical Magazine*, **59**, 341–347.

Momma K. and Izumi F. (2011) VESTA 3 for three-dimensional visualization of crystal, volumetric and morphology data. *Journal of Applied Crystallography*, **44**, 1272–1276.

Moore P.B. (1970) Mineralogy & chemistry of Långban-type deposits in Bergslagen, Sweden. *The Mineralogical Record*, **1**, 154–172.

Nysten P., Holtstam D. and Jonsson E. (1999) The Långban minerals. Pp. 89–183 in: *Långban: the Mines their Minerals Geology and Explorers* (D. Holtstam and J. Langhof, editors). Raster Förlag, Stockholm.

Palatinus L. and Chapuis G. (2007) SUPERFLIP – a computer program for the solution of crystal structures by charge flipping in arbitrary dimensions. *Journal of Applied Crystallography*, **41**, 786–790.

Petříček V., Dušek M. and Palatinus L. (2014) Crystallographic Computing System JANA2006: General features. *Zeitschrift für Kristallographie – Crystalline Materials*, **229**, 345–352.

Robinson K., Gibbs G.V. and Ribbe P.H. (1971) Quadratic elongation: a quantitative measure of distortion in coordination polyhedra. *Science*, **172**, 567–70.

Rumsey M.S., Welch M.D., Kleppe A.K. and Spratt J. (2017) Siidraite, $Pb_2Cu(OH)_2I_3$, from Broken Hill, New South Wales, Australia: the third halocuprate(I) mineral. *European Journal of Mineralogy*, **29**, 1027–1030.

Sheldrick G.M. (2015) Crystal structure refinement with SHELXL, *Acta Crystallographica*, **C71**, 3–8.

Venetopoulos C.Ch. and Rentzeperis P.J. (1975) The crystal structure of laurionite, $Pb(OH)Cl$. *Zeitschrift für Kristallographie*, **141**, 246–259.

Wang H., Chen H.-H, Borrmann H., Zhang Z.-J. and Zhao J.-T. (2012) Crystal growth and characterization of new-type lead tungstate single crystal. *Journal of Alloys and Compounds*, **545**, 135–138.

Yang X. and Huang J. (2012) Phase transformation of lead tungstate at normal temperature from tetragonal structure to monoclinic structure. *Journal of the American Ceramic Society*, **95**, 3334–3338.